Enhancing Perovskite Solar Cell Performance by Interface Engineering Using $CH_3NH_3PbBr_{0.9}I_{2.1}$ Quantum Dots

Mingyang Cha,[†,§] Peimei Da,[†,§] Jun Wang,[‡] Weiyi Wang,[‡] Zhanghai Chen,[‡] Faxian Xiu,[‡] Gengfeng Zheng,*[,†] and Zhong-Sheng Wang*[,†]

[†]Department of Chemistry, Laboratory of Advanced Materials, Collaborative Innovation Center of Chemistry for Energy Materials, Fudan University, 2205 Songhu Road, Shanghai 200438, China

[‡]State Key Laboratory of Surface Physics, Key Laboratory of Micro and Nano Photonic Structures (Ministry of Education), Department of Physics, Collaborative Innovation Center of Advanced Microstructures, Fudan University, 220 Handan Road, Shanghai 200433, China

ⓢ *Supporting Information*
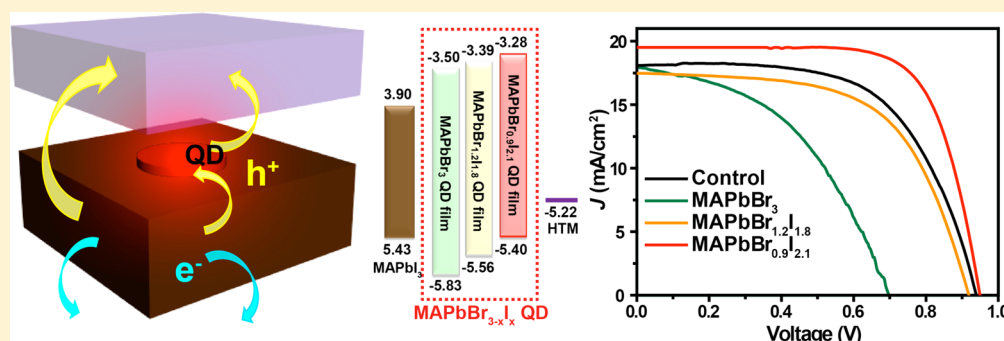
ABSTRACT: To improve the interfacial charge transfer that is crucial to the performance of perovskite solar cells, the interface engineering in a device should be rationally designed. Here we have developed an interface engineering method to tune the photovoltaic performance of planar-heterojunction perovskite solar cells by incorporating $MAPbBr_{3-x}I_x$ (MA = CH_3NH_3) quantum dots (QDs) between the $MAPbI_3$ perovskite film and the hole-transporting material (HTM) layer. By adjustment of the Br:I ratio, the as-synthesized $MAPbBr_{3-x}I_x$ QDs show tunable fluorescence and band edge positions. When the valence band (VB) edge of $MAPbBr_{3-x}I_x$ QDs is located below that of the $MAPbI_3$ perovskite, the hole transfer from the $MAPbI_3$ perovskite film to the HTM layer is hindered, and hence, the power conversion efficiency decreases. In contrast, when the VB edge of $MAPbBr_{3-x}I_x$ QDs is located between the VB edge of the $MAPbI_3$ perovskite film and the highest occupied molecular orbital of the HTM layer, the hole transfer from the $MAPbI_3$ perovskite film to the HTM layer is well-facilitated, resulting in significant improvements in the fill factor, short-circuit photocurrent, and power conversion efficiency.

INTRODUCTION

Organic–inorganic hybrid perovskite materials have recently gained substantial attention because of their high efficiency, low cost, superior optical properties, and all-solution-process fabrication.[1−7] The most attractive and representative perovskites are methylammonium lead halides ($CH_3NH_3PbX_3$, denoted as $MAPbX_3$, X = Br, Cl, I), which were discovered in 2009 as sensitizers in dye-sensitized solar cells (DSSCs).[8] To date, perovskite solar cells (PSCs) with methylammonium lead halide have achieved a power conversion efficiency (PCE) of 19.3%,[9] and an efficiency exceeding 20% has recently been obtained by replacing methylammonium with formamidinium.[10] In spite of these exciting ongoing developments, the interfacial charge transfer processes are still to be optimized. Several routes have been explored to facilitate the electron transfer, such as the insertion of an ultrathin electron extraction layer of graphene quantum dots (QDs) between the perovskite and TiO_2[11] and the incorporation of ZnO/reduced graphene

oxide QDs as an electron transfer layer.[12] Recently, PbS QDs have been introduced into planar PSCs as an effective inorganic p-type hole-transporting material (HTM) with appropriate energy alignment,[13,14] and the absorption of PbS QDs also extends the whole absorption spectrum of PSCs into the infrared region.[13]

Although QDs have been applied in various solar cell structures because of their high absorption coefficients and tunable energy levels,[15−21] engineering of the energy band alignment of QDs between the perovskite and HTM is also highly intriguing and has yet to be unraveled. In addition, compared with facilitating electron transport, the realization of an optimized interface between the perovskite and HTM for hole transfer is even more challenging, as the material synthesis and processing steps should fit with the stability requirements
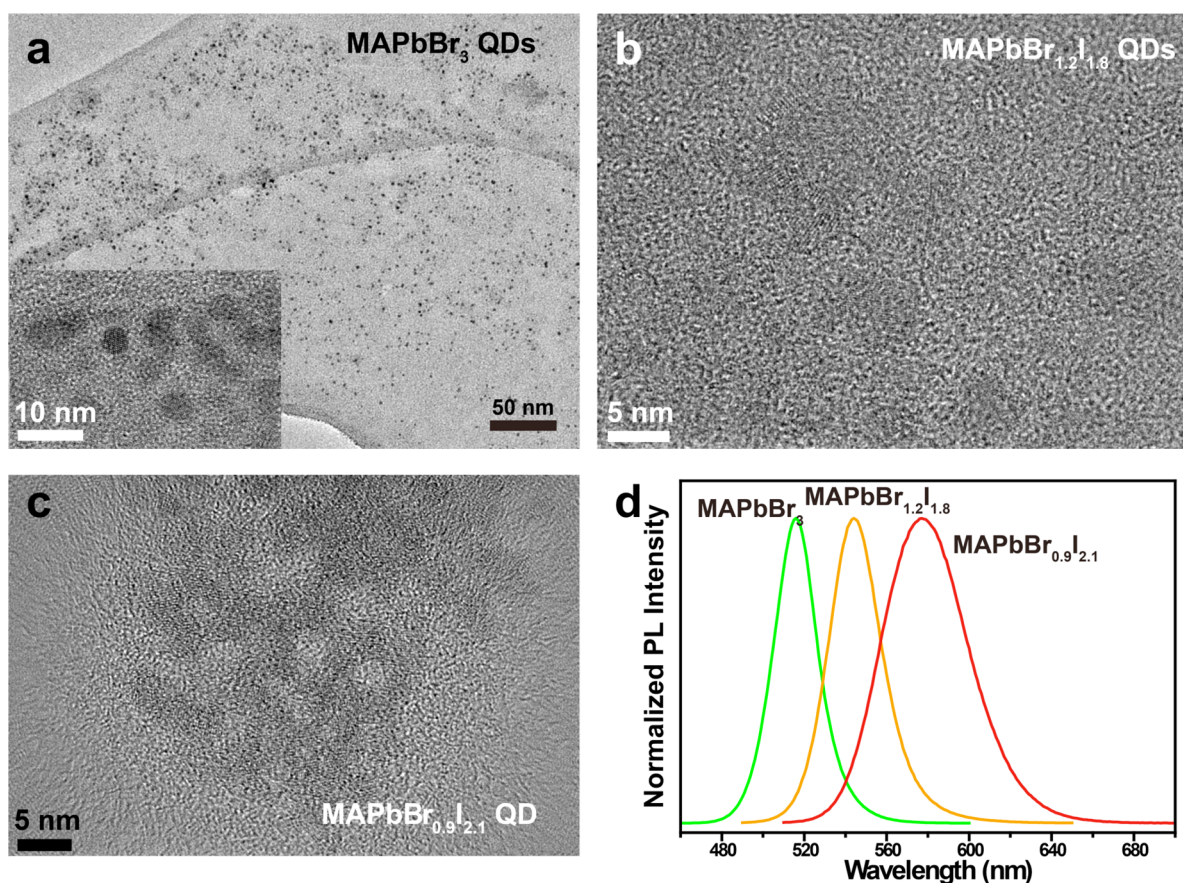
Figure 1. (a−c) TEM images of (a) MAPbBr$_3$, (b) MAPbBr$_{1.2}$I$_{1.8}$, and (c) MAPbBr$_{0.9}$I$_{2.1}$ QDs. (d) Photoluminescence spectra of MAPbBr$_{3-x}$I$_x$ QD solutions with an excitation wavelength of 400 nm.
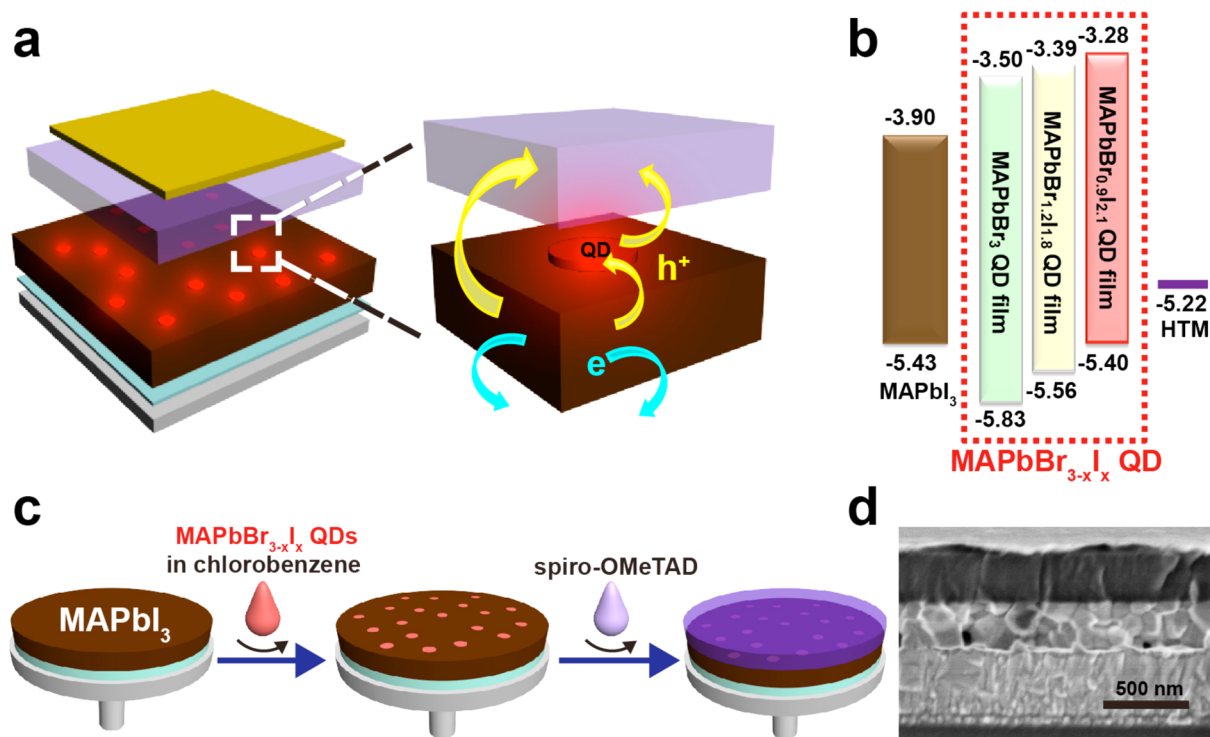

Figure 2. (a) Schematic illustration of the perovskite solar cell device structure. (b) Energy diagram of each material in the perovskite solar cell device, with energy levels given in eV. (c) Schematic illustration of the fabrication procedures for the perovskite solar cells with MAPbBr$_{3-x}$I$_x$ QDs. (d) Cross-sectional SEM image of a device.
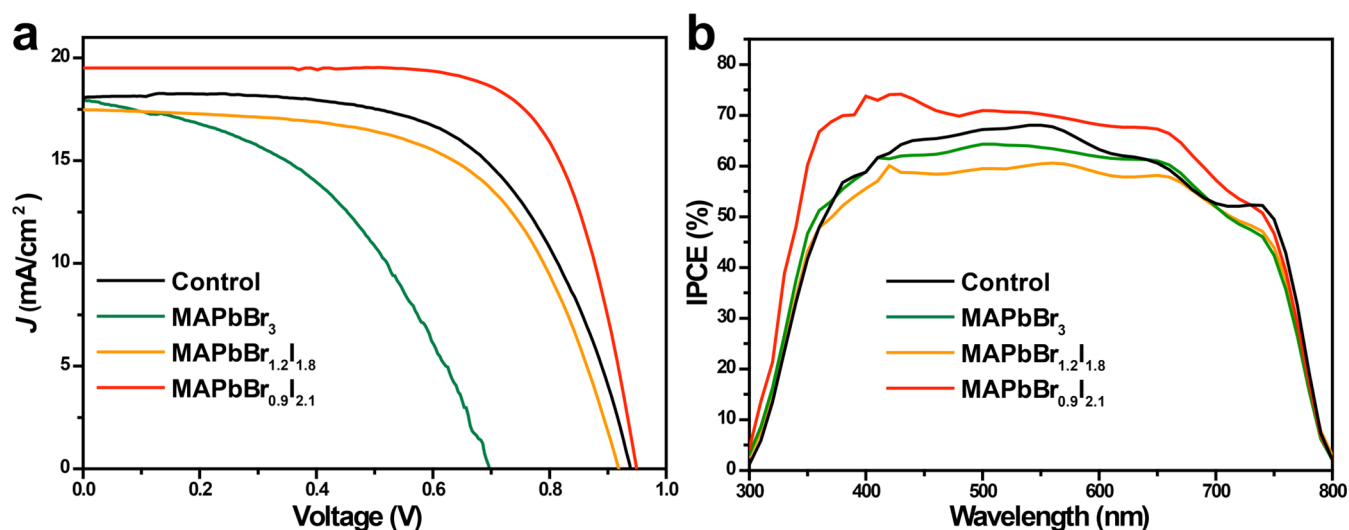
Figure 3. (a) *J*−*V* curves and (b) IPCE spectra of PSCs employing MAPbBr$_{3-x}$I$_x$ QDs as the interface-regulating material.

Table 1. Photovoltaic Parameters of Various Solar Cells

device	V_{oc} (mV)	J_{sc} (mA cm^{-2})	FF	PCE (%)
MAPbI$_3$/HTM (control)	937	18.09	0.61	10.34
MAPbI$_3$/MAPbBr$_3$-QDs/HTM	698	17.93	0.45	5.63
MAPbI$_3$/MAPbBr$_{1.2}$I$_{1.8}$-QDs/HTM	918	17.50	0.60	9.64
MAPbI$_3$/MAPbBr$_{0.9}$I$_{2.1}$-QDs/HTM	948	19.51	0.72	13.32

of the underlying perovskite layer without introducing any subsequent structural deterioration. The recently developed organometallic halide perovskite QDs have shown high photoluminescence (PL) quantum yields and low excitation energies.[22−24] Furthermore, perovskite QDs have lattice constants and processing requirements similar to those of planar perovskite layers. These results suggest that organometallic halide perovskite QDs have great potential for interface engineering in PSCs due to their tunable energy bands.

Inspired by these promises, herein we demonstrate rationally designed interface engineering of PSCs with composition-tailorable organometallic halide perovskite QDs for optimized band alignment and photoelectric conversion enhancement. A series of organometallic halide perovskite QDs with various Br:I ratios were synthesized and incorporated between the MAPbI$_3$ perovskite and HTM (i.e., spiro-OMeTAD) layers for interface engineering. The photogenerated holes in the perovskite layer were efficiently extracted to the HTM layer with the assistance of MAPbBr$_{0.9}$I$_{2.1}$ QDs, as revealed by the increased charge carrier lifetime and reduced charge transfer resistance over the interface. A notable 29% increase in PCE from 10.34% to 13.32% was thus obtained, suggesting that this approach is a promising means for interface engineering toward efficient charge carrier extraction and hence high photovoltaic performance.

■ RESULTS AND DISCUSSION

A series of MAPbBr$_{3-x}$I$_x$ QDs were synthesized in anhydrous chlorobenzene with *n*-octylamine as the coligand and stabilizer[22] (Figure S1 and Methods in the Supporting Information). Figure 1a−c displays transmission electron microscopy (TEM) images of MAPbBr$_3$, MAPbBr$_{1.2}$I$_{1.8}$, and MAPbBr$_{0.9}$I$_{2.1}$ QDs, respectively. These QDs have an average diameter of 5 nm with excellent homogeneity. Figure 1d shows

the PL spectra of these QD solutions. Interestingly, the emission peak can be finely tuned from 515 to 580 nm by varying the Br:I atomic ratio from 3:0 to 0.9:2.1. The emission peak gradually shifts to longer wavelength with decreasing Br:I ratio in the QD, which is ascribed to the larger iodide-atom-induced structural deviation from the cubic phase.[22]

The synthesized MAPbBr$_{3-x}$I$_x$ QDs were used to modify the interface between the MAPbI$_3$ perovskite film and the HTM layer, and a MAPbI$_3$/QDs/HTM device structure (Figure 2a) was proposed and investigated in this work. To determine the energy levels of MAPbBr$_{3-x}$I$_x$ QDs, UV−vis absorption spectroscopy and UV photoelectron spectroscopy (UPS) were performed (see Methods in the Supporting Information). The UV−vis absorption spectra of the QD solutions reveal that the gaps between the conduction band (CB) edge and the valence band (VB) edge, as determined by the wavelength of onset absorption (Figure S2), are 2.33, 2.17, and 2.12 eV for MAPbBr$_3$, MAPbBr$_{1.2}$I$_{1.8}$, and MAPbBr$_{0.9}$I$_{2.1}$, respectively. The VB edges, as determined by UPS (Figure S3), are −5.83, −5.56, and −5.40 eV for MAPbBr$_3$, MAPbBr$_{1.2}$I$_{1.8}$, and MAPbBr$_{0.9}$I$_{2.1}$ QDs, respectively. The CB edges, calculated using the expression CB = VB + energy gap, are −3.50, −3.39, and −3.28 eV for MAPbBr$_3$, MAPbBr$_{1.2}$I$_{1.8}$, and MAPbBr$_{0.9}$I$_{2.1}$, respectively. The schematic energy level diagram of the perovskite, MAPbBr$_{3-x}$I$_x$ QDs, and HTM is displayed in Figure 2b.

Evidently, changing the Br:I ratio in the QDs can successfully tune the energy levels, which are quite different from those of the perovskite film. The VB edge of MAPbBr$_{0.9}$I$_{2.1}$ lies between the VB of MAPbI$_3$ perovskite and the highest occupied molecular orbital (HOMO) of the HTM, which can facilitate the hole transfer at the interface. In contrast, the VB edges of the other two QDs are located below that of MAPbI$_3$ perovskite, which may hinder the interfacial hole transfer.

Table 2. Average Photovoltaic Parameters of Various Solar Cells

device	V_{oc} (mV)	J_{sc} (mA cm^{-2})	FF	PCE (%)
MAPbI$_3$/HTM (control)	880 ± 53	18.02 ± 0.42	0.59 ± 0.03	9.38 ± 0.71
MAPbI$_3$/MAPbBr$_3$-QDs/HTM	715 ± 49	17.95 ± 0.22	0.42 ± 0.04	5.12 ± 0.38
MAPbI$_3$/MAPbBr$_{1.2}$I$_{1.8}$-QDs/HTM	771 ± 129	17.94 ± 2.17	0.54 ± 0.06	8.69 ± 0.82
MAPbI$_3$/MAPbBr$_{0.9}$I$_{2.1}$-QDs/HTM	913 ± 30	18.62 ± 1.14	0.70 ± 0.05	12.03 ± 0.99

The PSC devices were fabricated by spin coating of QDs onto the surface of the MAPbI$_3$ perovskite film while keeping other steps the same as those in the planar MAPbI$_3$/HTM structure[25] (Figure 2c and Methods in the Supporting Information). Generally, the optimized device structure consisted of a 50 nm thick dense TiO$_2$ layer on fluorine-doped tin oxide (FTO), a 320 nm thick perovskite layer, a 250 nm thick spiro-OMeTAD layer, and a magnetron-sputtered Au layer (80 nm) as the back contact,[26] as shown in the cross-sectional scanning electron microscopy (SEM) image in Figure 2d.

The current−voltage (J−V) curves for the best PSC devices with different MAPbBr$_{3−x}$I$_x$ QDs are shown in Figure 3a, and the photovoltaic performance parameters are summarized in Table 1. Upon introduction of MAPbBr$_{3−x}$I$_x$ QDs, the photovoltaic performance changed significantly, depending on the Br:I ratio. The best control cell (MAPbI$_3$/HTM) produced an open-circuit photovoltage (V_{oc}) of 937 mV, a short-circuit photocurrent density (J_{sc}) of 18.09 mA cm^{-2}, and a fill factor (FF) of 0.61, corresponding to a PCE of 10.34%. On the other hand, the introduction of MAPbBr$_3$ QDs at the MAPbI$_3$−HTM interface decreased the PCE remarkably to 5.63% because of the significant decreases in V_{oc} and FF compared with the control cell. Decreasing the Br:I ratio to 1.2:1.8 using the MAPbBr$_{1.2}$I$_{1.8}$ QDs resulted in a PCE of 9.64%, which was slightly lower than the efficiency of the control device. Interestingly, when the Br:I ratio was further decreased to 0.9:2.1, the MAPbI$_3$/MAPbBr$_{0.9}$I$_{2.1}$-QDs/HTM device produced a V_{oc} of 948 mV, a J_{sc} of 19.51 mA cm^{-2}, and an FF of 0.72, corresponding to a PCE of 13.32%. The enhancement of PCE is attributed to the significant improvement in J_{sc} and FF as well as the slight increase in V_{oc}. The PCE increased with decreasing Br:I ratio up to 0.9/2.1 for the MAPbI$_3$/MAPbBr$_{3−x}$I$_x$-QDs/HTM devices.

Figure 3b shows the incident photon-to-current conversion efficiency (IPCE) of each cell. The maximum IPCE increases in the order MAPbBr$_3$ < MAPbBr$_{1.2}$I$_{1.8}$ < control < MAPbBr$_{0.9}$I$_{2.1}$, in good agreement with the J_{sc} trend. Compared with the control cell, the introduction of MAPbBr$_3$ or MAPbBr$_{1.2}$I$_{1.8}$ QDs with a lower VB edge at the MAPbI$_3$−HTM interface hinders the photoelectric conversion, while incorporating the MAPbBr$_{0.9}$I$_{2.1}$ QDs with a slightly higher VB edge at the MAPbI$_3$−HTM interface improves the IPCE. The MAPbI$_3$/MAPbBr$_{0.9}$I$_{2.1}$-QDs/HTM device shows the best IPCE performance among the four cells, accounting for its highest J_{sc}.

The thickness of the MAPbBr$_{0.9}$I$_{2.1}$ QDs may influence the performance of PSCs greatly, but it was too thin to detect because of the pretty small amount of QDs deposited on the perovskite surface. Figure S4 shows top-view SEM images of the perovskite film before and after deposition of MAPbBr$_{0.9}$I$_{2.1}$ QDs. Because of the tiny size of the QDs and quite small loading, the change in the surface morphology was negligible and the QDs were hardly observed. It was thus impossible to obtain thickness information on MAPbBr$_{0.9}$I$_{2.1}$ QDs. Instead, the influence of the number of spin coatings and the

concentration of MAPbBr$_{0.9}$I$_{2.1}$ QDs on the performance of PSCs was investigated. The amount of MAPbBr$_{0.9}$I$_{2.1}$ QDs deposited on the MAPbI$_3$ perovskite film was tuned by changing the concentration of the MAPbBr$_{0.9}$I$_{2.1}$ QD suspension and by varying the number of spin coatings. Qualitatively, the amount of MAPbBr$_{0.9}$I$_{2.1}$ QDs influences the photovoltaic performance significantly (Table S1). It was found that spin coating of 0.32 mM MAPbBr$_{0.9}$I$_{2.1}$ QDs one time produced the best performance in our experiments. All of the PSC devices interfaced with the MAPbBr$_{3−x}$I$_x$ QDs in this work were fabricated under these optimized conditions.

To examine the reproducibility of photovoltaic performance, six parallel samples for each PSC structure were fabricated and evaluated in terms of photovoltaic performance. The average photovoltaic performance parameters are summarized in Table 2. The average PCE for the typical planar MAPbI$_3$/HTM device obtained in this work was 9.38%. When MAPbBr$_{3−x}$I$_x$ QDs were deposited on top of the perovskite film, the average PCE values were 5.12%, 8.69%, and 12.03% for MAPbBr$_3$, MAPbBr$_{1.2}$I$_{1.8}$, and MAPbBr$_{0.9}$I$_{2.1}$ QDs, respectively. The change trend for each average parameter is consistent with that for each best parameter.

If the Br:I ratio in the QD is decreased further, how does the performance of the PSCs change? To address this question, two more types of QDs were prepared: MAPbBr$_{0.7}$I$_{2.3}$ and MAPbBr$_{0.4}$I$_{2.6}$ QDs (Methods in the Supporting Information). However, the PSCs interfaced with the MAPbBr$_{0.7}$I$_{2.3}$ or MAPbBr$_{0.4}$I$_{2.6}$ QDs showed lower performance than that with the MAPbBr$_{0.9}$I$_{2.1}$ QDs (Table S2). Therefore, further decreasing the Br:I ratio leads to decreased photovoltaic performance. The emission peaks of the MAPbBr$_{0.7}$I$_{2.3}$ and MAPbBr$_{0.4}$I$_{2.6}$ QD solutions are located at 624 and 655 nm, respectively (Figure S5). Compared with the previously mentioned three QDs, further red shifts of the emission peak are achieved since the Br:I ratio is further reduced. Since the MAPbBr$_{0.7}$I$_{2.3}$ and MAPbBr$_{0.4}$I$_{2.6}$ QDs have poor stability due to the lower Br:I ratio,[22] the two QDs were not investigated in detail in this work.

To investigate the stability of the PSC devices, the photovoltaic performance of the PSCs was measured every other day for 25 days. The evolution of the PCE with time is displayed in Figure S6. The initial PCE of the PSC without the MAPbBr$_{0.9}$I$_{2.1}$ QDs was 10.07%, and the PCE decreased to 8.17% after 25 days, corresponding to an attenuation of 19%. By contrast, the PSC with the MAPbBr$_{0.9}$I$_{2.1}$ QDs experienced a PCE drop of 17% (from 12.55% to 10.37%) after 25 days. Thus, the PSCs with and without MAPbBr$_{0.9}$I$_{2.1}$ QDs have similar stability.

Next, the factors that influence the photovoltaic performance of the PSCs were analyzed. The photocurrent generation is directly related to the light-harvesting efficiency. The fluorescence of MAPbBr$_{3−x}$I$_x$ QDs may enhance the light-harvesting by the active layer, as the emitted photons can be absorbed by the perovskite film. However, this case does not apply in our experiments, as the UV−vis absorption spectra for
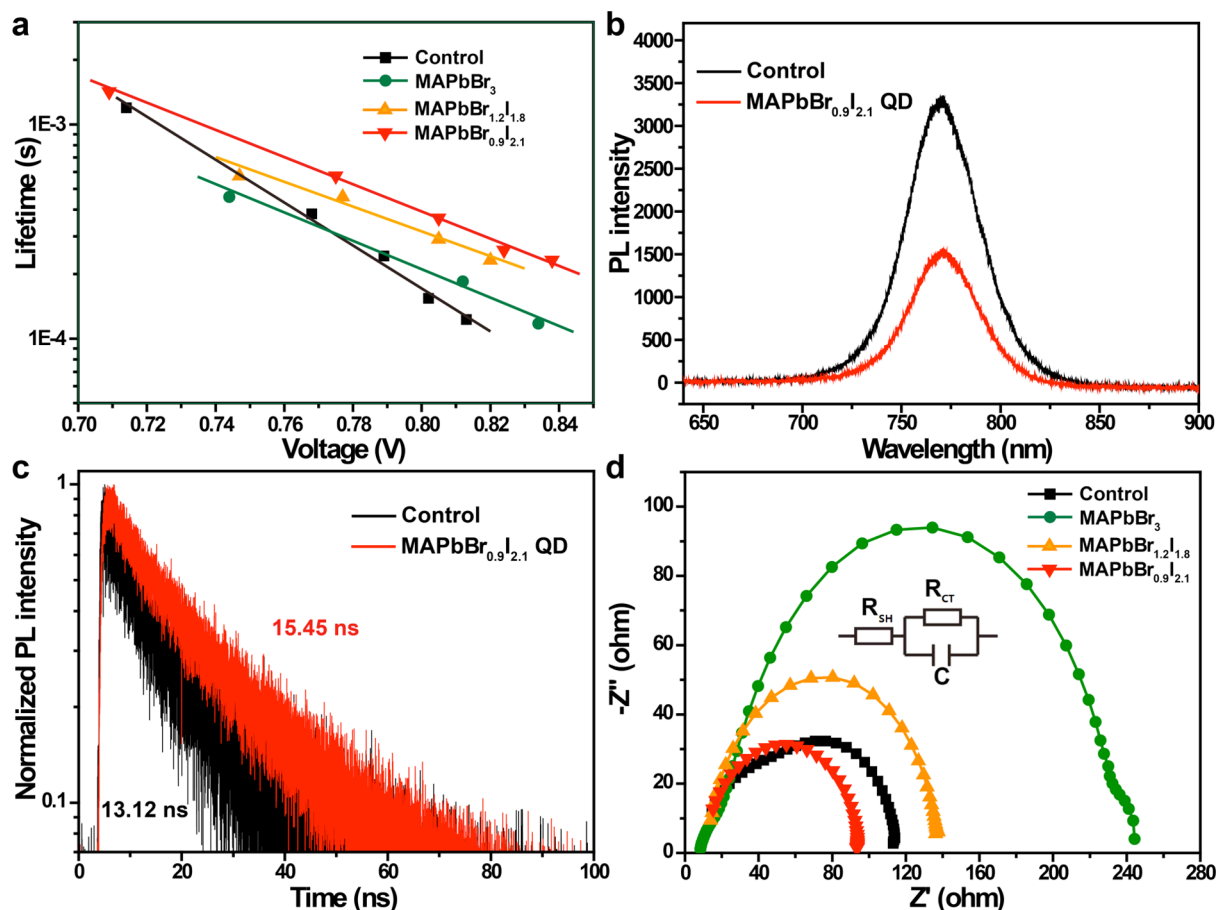
Figure 4. (a) Electron lifetimes measured by IMVS for various PSCs. (b) Photoluminescence spectra and (c) time-resolved photoluminescence decay curves of $MAPbI_3$ (control) and $MAPbI_3/MAPbBr_{0.9}I_{2.1}$-QDs perovskite films. (d) Electrochemical impedance responses of PSCs measured at open circuit under AM 1.5G simulated sunlight.

the perovskite films with and without $MAPbBr_{3-x}I_x$ QDs are similar (Figure S7). As the PSC devices are illuminated from the FTO side, most of the incident visible light is absorbed by the $MAPbI_3$ perovskite film, so the $MAPbBr_{3-x}I_x$ QDs are difficult to excite to elicit fluorescence. In addition, because the amount of $MAPbBr_{3-x}I_x$ QDs on the active layer is pretty small, the fluorescence and light absorption of the $MAPbBr_{3-x}I_x$ QDs at the interface are negligible. Therefore, the fluorescence characteristics and light absorption properties of $MAPbBr_{3-x}I_x$ QDs do not affect the light harvesting by the active layer in this case. As the light-harvesting efficiencies of the films are similar, the observed difference in performance should be attributed to the modification of $MAPbI_3$–HTM interface by the $MAPbBr_{3-x}I_x$ QDs. The $MAPbBr_3$ QDs have a much lower VB edge than the $MAPbI_3$ perovskite, which hinders the hole transfer from the perovskite film to the HTM layer, leading to significant decreases in V_{oc}, FF, and PCE.[13] As the $MAPbBr_{1.2}I_{1.8}$ QDs have slightly lower VB edge than the $MAPbI_3$ perovskite, the blocking effect on the hole transfer diminishes, resulting in slightly decreased V_{oc}, FF, and PCE. Compared with the control cell, the decreases in V_{oc} and FF become more prominent as the VB edge is lowered because of the enhanced blocking effect on hole transfer.

However, the VB edge of $MAPbBr_{0.9}I_{2.1}$ QDs is located between the VB edge of the $MAPbI_3$ perovskite film and the HOMO of the HTM (Figure 2b). In this situation, the photogenerated holes in the perovskite film produced by

irradiation may first transfer to the $MAPbBr_{0.9}I_{2.1}$ QDs and then to the HTM layer. The two-step hole transfer resulting from such interface engineering facilitates the hole transfer from the perovskite film to the HTM layer[27] as a result of the better matching of energy levels among the perovskite, $MAPbBr_{0.9}I_{2.1}$ QDs, and HTM. As a consequence, J_{sc}, V_{oc} and FF all are enhanced, resulting in a significant improvement in the PCE.

For comparison, the effect of QDs embedded in the $MAPbI_3$ perovskite layer on the photovoltaic performance was also examined. The $MAPbI_3$–$MAPbBr_{3-x}I_x$-QDs mixed layer was fabricated by adding $MAPbBr_{3-x}I_x$ QDs into the antisolvent chlorobenzene[25] during the one-step spin coating of $MAPbI_3$ perovskite, as shown in the schematic illustration of the fabrication process (Figure S8). The $MAPbBr_{0.9}I_{2.1}$ QDs inside the $MAPbI_3$ layer produced a PCE of only 6.93% (Table S3), and the results of mixing the other two QDs were even worse. The inferior performance is attributed to the existence of a large number of recombination spots due to the difference between the VB levels of the QDs and perovskite, which limits the hole transport through the mixed layer. These results indicate that it is essential to introduce $MAPbBr_{0.9}I_{2.1}$ QDs at the $MAPbI_3$–HTM interface to obtain high performance.

To further explore the influence of $MAPbBr_{3-x}I_x$ QDs on the photovoltaic performance, the PSC devices were characterized by intensity-modulated photovoltage spectroscopy (IMVS).[28,29] Figure 4a shows the electron lifetime (τ_n) derived from the IMVS measurement versus the applied potential. For all of the

PSCs, the logarithm of the electron lifetime decreases linearly with the applied potential. At the same bias potential, the electron lifetimes increase in the order $MAPbBr_3$ < $MAPbBr_{1.2}I_{1.8}$ < $MAPbBr_{0.9}I_{2.1}$, in good agreement with the V_{oc} sequence. As the lower VB edges of $MAPbBr_3$ and $MAPbBr_{1.2}I_{1.8}$ compared with that of the $MAPbI_3$ perovskite hinder hole extraction to the HTM layer, the electron−hole recombination probability increases, leading to a shorter electron lifetime. However, for the $MAPbBr_{0.9}I_{2.1}$ QDs with a VB edge located between that of the perovskite film and the HOMO of the HTM layer, the photogenerated holes in the perovskite film can first transfer to the $MAPbBr_{0.9}I_{2.1}$ QDs and then to the HTM layer.[27] This is favorable for faster hole extraction, and it is therefore reasonable to get a longer electron lifetime for this case. As a result of the best hole extraction, the highest J_{sc}, V_{oc}, FF, and PCE are obtained for the $MAPbBr_{0.9}I_{2.1}$ QDs.

The steady-state PL spectra (Figure 4b) were recorded in order to gain insight into the defect density of the perovskite films with and without $MAPbBr_{0.9}I_{2.1}$ QDs. Surface modification of the $MAPbI_3$ perovskite film with $MAPbBr_{0.9}I_{2.1}$ QDs exhibits an obvious PL quenching (Figure 4b). The decreased PL intensity indicates that the introduction of $MAPbBr_{0.9}I_{2.1}$ QDs reduces the defect density of the perovskite film. Moreover, the time-resolved PL decay curves of the $MAPbI_3$ and $MAPbI_3/MAPbBr_{0.9}I_{2.1}$-QDs were measured to determine the PL decay lifetimes (Figure 4c). The PL decay curves were fitted by the single-exponential decay function $I = Ae^{-(t-t_0)/\tau_1}$,[30] in which I is the PL intensity at time t, A is a constant, and τ_1 is the faster component of the exciton spontaneous radiative recombination time. The PL decay lifetime of the perovskite film interfaced with $MAPbBr_{0.9}I_{2.1}$ QDs was determined to be 15.45 ns, compared with 13.12 ns for the control film without QDs. Since there is no HTM layer in the sample, the PL decay is attributed not to carrier extraction by the HTM layer but rather to radiative and nonradiative deexcitation.[9] The prolonged PL decay lifetime of the perovskite film covered with $MAPbBr_{0.9}I_{2.1}$ QDs is the result of suppressed nonradiative recombination channels.[9] The longer PL lifetime suggests slower charge recombination for the film with $MAPbBr_{0.9}I_{2.1}$ QDs.[9,31] Upon excitation, the photogenerated holes in the perovskite film can transfer to the $MAPbBr_{0.9}I_{2.1}$ QDs with higher VB, causing electrons and holes to be located at different phases. The effective separation of electrons and holes retards the charge recombination and thus enhances the PL lifetime. For comparison, the PL lifetime of $MAPbI_3−MAPbBr_{0.9}I_{2.1}$-QDs fabricated by mixing $MAPbBr_{0.9}I_{2.1}$ QDs inside the $MAPbI_3$ layer was also measured (Figure S9) and fitted by the double-exponential decay function $I = Ae^{-(t-t_0)/\tau_1} + Be^{-(t-t_0)/\tau_2}$,[30] where τ_2 is the slower component of the pure dephasing time of nonradiative recombination, such as the phonon scattering and Auger recombination losses.[31] The mixed $MAPbI_3−MAPbBr_{0.9}I_{2.1}$-QDs layer showed a τ_1 of 7.23 ns, which is much smaller than that of the $MAPbI_3/MAPbBr_{0.9}I_{2.1}$-QDs layer and that of the control film as well. These results further indicate that employing the $MAPbBr_{0.9}I_{2.1}$ QDs as an interface-regulating material rather than an additive inside the perovskite film is crucial to achieve high photovoltaic performance.

To clarify the significant changes in FF caused by the $MAPbBr_{3−x}I_x$ QDs, electrochemical impedance spectroscopy (EIS) was carried out. Figure 4d shows the Nyquist spectra of PSCs with and without $MAPbBr_{3−x}I_x$ QDs under one-sun illumination in the frequency range between 1 MHz and 0.1 Hz along with the equivalent circuit (Figure 4d inset). Only one semicircle is resolved in the EIS spectra, which describes the charge transfer behavior at the $MAPbI_3$−HTM interface. The intercept of the semicircle on the real axis corresponds to the series resistance (R_s), which largely depends on the FTO substrate and external wire contact. The values of R_s are similar for these PSCs, excluding the effect of R_s on the FF. R_{ct} represents the charge transfer resistance at the $MAPbI_3$−HTM interface, and C is the corresponding capacitance. The value of R_{ct} changes greatly when the $MAPbBr_{3−x}I_x$ QDs are introduced. For PSCs with $MAPbBr_3$ and $MAPbBr_{1.2}I_{1.8}$ QDs, R_{ct} increases, suggesting that the hole extraction becomes less efficient compared with the control device. This is the case because the lowering of the VB edge hinders the hole transfer from the $MAPbI_3$ perovskite film to the HTM layer. The decrease in FF for $MAPbBr_3$ and $MAPbBr_{1.2}I_{1.8}$ QDs is attributed to the increased R_{ct}. For the $MAPbBr_{0.9}I_{2.1}$ QD-interfaced PSC, R_{ct} decreases, indicating that hole extraction becomes more efficient compared with the control cell. The VB of $MAPbBr_{0.9}I_{2.1}$ QDs lies between the VB of $MAPbI_3$ and the HOMO of the HTM, facilitating the hole transfer from the $MAPbI_3$ perovskite to the HTM and thus decreasing R_{ct}, which is responsible for the increase in FF. These results indicate that $MAPbBr_{0.9}I_{2.1}$ QDs at the interface can enhance charge separation, thus improving the FF and PCE.[32]

■ CONCLUSIONS

We have developed planar-heterojunction perovskite solar cells employing $MAPbBr_{3−x}I_x$ QDs as the interface-regulating materials. Hole transfer from the $MAPbI_3$ perovskite into the HTM layer is favored by $MAPbBr_{0.9}I_{2.1}$ QDs with a suitable VB edge but hindered by $MAPbBr_3$ and $MAPbBr_{1.2}I_{1.8}$ QDs with VB edges lower than that of the perovskite film. The interfacial modification with the $MAPbBr_{0.9}I_{2.1}$ QDs improves the hole extraction and thus enhances the FF, J_{sc}, and PCE significantly. This work may inspire new mechanisms for interface modulation in PSCs toward higher performance.

■ ASSOCIATED CONTENT

ⓈSupporting Information

The Supporting Information is available free of charge on the ACS Publications website at DOI: 10.1021/jacs.6b04519.

> Methods; additional figures showing the reaction system, UV−vis spectra for quantum dot solutions, UPS of quantum dot films, top-view SEM images of perovskite films before and after deposition of quantum dots, PL spectra of QD solutions, stability of PSCs, UV−vis spectra of quantum-dot-deposited perovskite films, fabrication process of mixing quantum dots inside the perovskite layer, PL decay curves of perovskite films mixed with quantum dots, and photographs of perovskite films; tables summarizing the photovoltaic performance of PSCs with various amounts of QDs, PSCs based on $MAPbBr_{0.7}I_{2.3}$ and $MAPbBr_{0.4}I_{2.6}$ QDs, and PSCs with QDs mixed in the perovskite film (PDF)

■ AUTHOR INFORMATION

Corresponding Authors

*zs.wang@fudan.edu.cn
*gfzheng@fudan.edu.cn

Author Contributions

§M.C. and P.D. contributed equally.

Notes

The authors declare no competing financial interest.

■ REFERENCES

(1) Burschka, J.; Pellet, N.; Moon, S.-J.; Humphry-Baker, R.; Gao, P.; Nazeeruddin, M. K.; Grätzel, M. *Nature* **2013**, *499*, 316−319.

(2) Hou, Y.; Zhang, H.; Chen, W.; Chen, S.; Quiroz, C. O. R.; Azimi, H.; Osvet, A.; Matt, G. J.; Zeira, E.; Seuring, J.; Kausch-Busies, N.; Lövenich, W.; Brabec, C. J. *Adv. Energy Mater.* **2015**, *5*, 1500543.

(3) Zhang, H.; Mao, J.; He, H.; Zhang, D.; Zhu, H. L.; Xie, F.; Wong, K. S.; Grätzel, M.; Choy, W. C. H. *Adv. Energy Mater.* **2015**, *5*, 1501354.

(4) Li, X.; Dar, M. I.; Yi, C.; Luo, J.; Tschumi, M.; Zakeeruddin, S. M.; Nazeeruddin, M. K.; Han, H.; Grätzel, M. *Nat. Chem.* **2015**, *7*, 703−711.

(5) Ke, W.; Fang, G.; Wan, J.; Tao, H.; Liu, Q.; Xiong, L.; Qin, P.; Wang, J.; Lei, H.; Yang, G.; Qin, M.; Zhao, X.; Yan, Y. *Nat. Commun.* **2015**, *6*, 6700.

(6) Kaltenbrunner, M.; Adam, G.; Głowacki, E. D.; Drack, M.; Schwödiauer, R.; Leonat, L.; Apaydin, D. H.; Groiss, H.; Scharber, M. C.; White, M. S.; Sariciftci, N. S.; Bauer, S. *Nat. Mater.* **2015**, *14*, 1032−1039.

(7) You, J.; Meng, L.; Song, T.-B.; Guo, T.-F.; Yang, Y. M.; Chang, W.-H.; Hong, Z.; Chen, H.; Zhou, H.; Chen, Q.; Liu, Y.; De Marco, N.; Yang, Y. *Nat. Nanotechnol.* **2016**, *11*, 75−81.

(8) Kojima, A.; Teshima, K.; Shirai, Y.; Miyasaka, T. *J. Am. Chem. Soc.* **2009**, *131*, 6050−6051.

(9) Zhou, H.; Chen, Q.; Li, G.; Luo, S.; Song, T.-b.; Duan, H.-S.; Hong, Z.; You, J.; Liu, Y.; Yang, Y. *Science* **2014**, *345*, 542−546.

(10) Yang, W. S.; Noh, J. H.; Jeon, N. J.; Kim, Y. C.; Ryu, S.; Seo, J.; Seok, S. I. *Science* **2015**, *348*, 1234−1237.

(11) Zhu, Z.; Ma, J.; Wang, Z.; Mu, C.; Fan, Z.; Du, L.; Bai, Y.; Fan, L.; Yan, H.; Phillips, D. L.; Yang, S. *J. Am. Chem. Soc.* **2014**, *136*, 3760−3763.

(12) Tavakoli, M. M.; Tavakoli, R.; Nourbakhsh, Z.; Waleed, A.; Virk, U. S.; Fan, Z. *Adv. Mater. Interfaces* **2016**, *3*, 1500790.

(13) Hu, L.; Wang, W.; Liu, H.; Peng, J.; Cao, H.; Shao, G.; Xia, Z.; Ma, W.; Tang, J. *J. Mater. Chem. A* **2015**, *3*, 515−518.

(14) Li, Y.; Zhu, J.; Huang, Y.; Wei, J.; Liu, F.; Shao, Z.; Hu, L.; Chen, S.; Yang, S.; Tang, J.; Yao, J.; Dai, S. *Nanoscale* **2015**, *7*, 9902−9907.

(15) Chuang, C.-H. M.; Brown, P. R.; Bulović, V.; Bawendi, M. G. *Nat. Mater.* **2014**, *13*, 796−801.

(16) Carlson, B.; Leschkies, K.; Aydil, E. S.; Zhu, X.-Y. *J. Phys. Chem. C* **2008**, *112*, 8419−8423.

(17) Congreve, D. N.; Lee, J.; Thompson, N. J.; Hontz, E.; Yost, S. R.; Reusswig, P. D.; Bahlke, M. E.; Reineke, S.; Van Voorhis, T.; Baldo, M. A. *Science* **2013**, *340*, 334−337.

(18) Kramer, I. J.; Sargent, E. H. *Chem. Rev.* **2013**, *114*, 863−882.

(19) Ma, W.; Luther, J. M.; Zheng, H.; Wu, Y.; Alivisatos, A. P. *Nano Lett.* **2009**, *9*, 1699−1703.

(20) Luther, J. M.; Law, M.; Beard, M. C.; Song, Q.; Reese, M. O.; Ellingson, R. J.; Nozik, A. J. *Nano Lett.* **2008**, *8*, 3488−3492.

(21) Zhao, N.; Osedach, T. P.; Chang, L.-Y.; Geyer, S. M.; Wanger, D.; Binda, M. T.; Arango, A. C.; Bawendi, M. G.; Bulovic, V. *ACS Nano* **2010**, *4*, 3743−3752.

(22) Zhang, F.; Zhong, H.; Chen, C.; Wu, X.-g.; Hu, X.; Huang, H.; Han, J.; Zou, B.; Dong, Y. *ACS Nano* **2015**, *9*, 4533−4542.

(23) Tian, Y.; Merdasa, A.; Peter, M.; Abdellah, M.; Zheng, K.; Ponseca, C. S., Jr; Pullerits, T.; Yartsev, A.; Sundström, V.; Scheblykin, I. G. *Nano Lett.* **2015**, *15*, 1603−1608.

(24) Nedelcu, G.; Protesescu, L.; Yakunin, S.; Bodnarchuk, M. I.; Grotevent, M. J.; Kovalenko, M. V. *Nano Lett.* **2015**, *15*, 5635−5640.

(25) Xiao, M.; Huang, F.; Huang, W.; Dkhissi, Y.; Zhu, Y.; Etheridge, J.; Gray-Weale, A.; Bach, U.; Cheng, Y. B.; Spiccia, L. *Angew. Chem.* **2014**, *126*, 10056−10061.

(26) Da, P.; Cha, M.; Sun, L.; Wu, Y.; Wang, Z.-S.; Zheng, G. *Nano Lett.* **2015**, *15*, 3452−3457.

(27) Lee, Y.-L.; Chi, C.-F.; Liau, S.-Y. *Chem. Mater.* **2010**, *22*, 922−927.

(28) Pockett, A.; Eperon, G. E.; Peltola, T.; Snaith, H. J.; Walker, A.; Peter, L. M.; Cameron, P. J. *J. Phys. Chem. C* **2015**, *119*, 3456−3465.

(29) Wang, J.; Mora-Seró, I.; Pan, Z.; Zhao, K.; Zhang, H.; Feng, Y.; Yang, G.; Zhong, X.; Bisquert, J. *J. Am. Chem. Soc.* **2013**, *135*, 15913−15922.

(30) Wang, J.; Cao, R.; Da, P.; Wang, Y.; Hu, T.; Wu, L.; Lu, J.; Shen, X.; Xu, F.; Zheng, G.; Chen, Z. *Appl. Phys. Lett.* **2016**, *108*, 022103.

(31) Li, S.-S.; Chang, C.-H.; Wang, Y.-C.; Lin, C.-W.; Wang, D.-Y.; Lin, J.-C.; Chen, C.-C.; Sheu, H.-S.; Chia, H.-C.; Wu, W.-R.; Jeng, U-S.; Liang, C.-T.; Sankar, R.; Chou, F.-C.; Chen, C.-W. *Energy Environ. Sci.* **2016**, *9*, 1282−1289.

(32) Dualeh, A.; Moehl, T.; Tétreault, N.; Teuscher, J.; Gao, P.; Nazeeruddin, M. K.; Grätzel, M. *ACS Nano* **2014**, *8*, 362−373.